MINIREVIEW

Molecular Machinery and Mechanism of Cell Secretion

BHANU P. JENA

Department of Physiology, Wayne State University School of Medicine, Detroit, Michigan 48201

Secretion occurs in all living cells and involves the delivery of intracellular products to the cell exterior. Secretory products are packaged and stored in membranous sacs or vesicles within the cell. When the cell needs to secrete these products, the secretory vesicles containing them dock and fuse at plasma membrane-associated supramolecular structures, called porosomes, to release their contents. Specialized cells for neurotransmission, enzyme secretion, or hormone release use a highly regulated secretory process. Similar to other fundamental cellular processes, cell secretion is precisely regulated. During secretion, swelling of secretory vesicles results in a build-up of intravesicular pressure, allowing expulsion of vesicular contents. The extent of vesicle swelling dictates the amount of vesicular contents expelled. The discovery of the porosome as the universal secretory machinery, its isolation, its structure and dynamics at nanometer resolution and in real time, and its biochemical composition and functional reconstitution into artificial lipid membrane have been determined. The molecular mechanism of secretory vesicle swelling and the fusion of opposing bilayers, that is, the fusion of secretory vesicle membrane at the base of the porosome membrane, have also been resolved. These findings reveal, for the first time, the universal molecular machinery and mechanism of secretion in cells. Exp Biol Med 230:307–319, 2005

Key words: secretion; membrane fusion; porosome or fusion pore

Introduction

Secretion and membrane fusion are fundamental cellular processes regulating endoplasmic reticulum (ER)-Golgi and Golgi-Golgi transport, plasma membrane recycling, cell division, sexual reproduction, acid secretion, histamine release, and the release of enzymes, hormones, and neurotransmitters, to name just a few. It is therefore no surprise that defects in secretion and membrane fusion lead to diabetes, Alzheimer's, Parkinson's, and a host of diseases. In view of this, there has been significant effort during the past half century to understand the molecular machinery and mechanism of secretion and membrane fusion in cells. Only in the last decade, studies using atomic force microscopy (AFM) and conventional biochemical, electrophysiological, and imaging approaches have provided a molecular understanding of these processes in cells (1–21). With these findings (1–21) made primarily in the author's laboratory, a new understanding of cell secretion has emerged. These studies further demonstrate secretory vesicles to transiently dock and fuse at the cell plasma membrane, which has been confirmed by a number of laboratories (22–27).

Throughout history, the development of new imaging tools has provided new insights into our perceptions of the living world and profoundly impacted human health. The invention of the light microscope, almost 300 years ago, was the first catalyst, propelling us into an era of modern biology and medicine. Using the light microscope, a giant step into the gates of modern biology and medicine was made with the discovery of the unit of life, the cell. The structure and morphology of normal and diseased cells and of disease-causing microorganisms were revealed for the first time using the light microscope. Then in 1938, with the birth of the electron microscope (EM), dawned a new era. Through the mid 1940s and 1950s, a number of subcellular organelles were discovered and their functions determined using the EM. Viruses, the new life forms, were identified and observed for the first time and implicated in diseases ranging from the common cold to autoimmune disease (AIDS). Despite the capability of the EM to image

Supported by grants DK-56212 and NS-39918 from the National Institutes of Health (B.P.J).

[1] To whom correspondence should be addressed at Department of Physiology, Wayne State University School of Medicine, 5239 Scott Hall, 540 E. Canfield Avenue, Detroit, MI 48201–4177. E-mail: bjena@med.wayne.edu

1535-3702/05/2305-0307$15.00

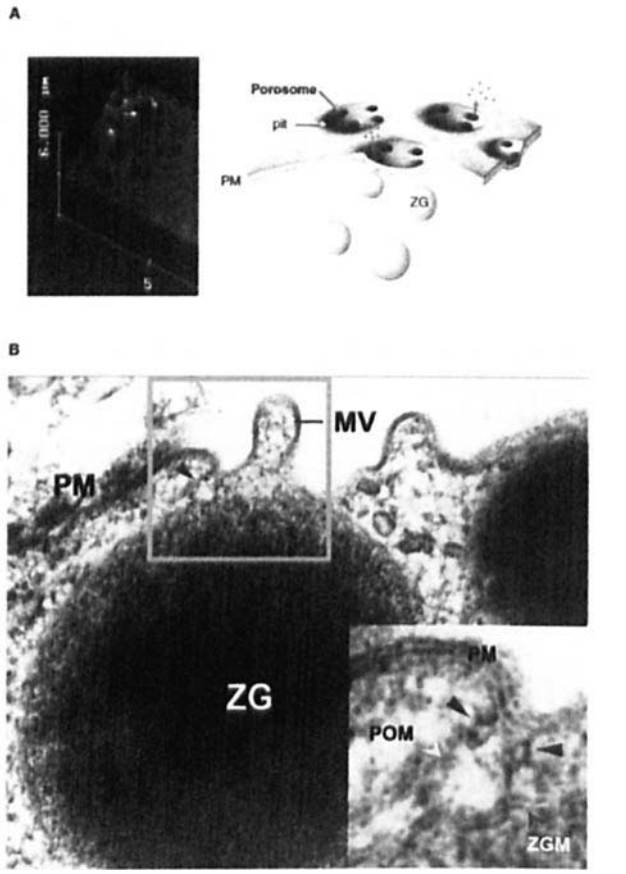

Figure 1. (A) On the far left is an AFM micrograph depicting pits (yellow arrow) and depressions within (blue arrow), at the plasma membrane in live pancreatic acinar cells. On the right is a schematic drawing depicting depressions, at the cell plasma membrane, where membrane-bound secretory vesicles dock and fuse to release vesicular contents (3). (B) Electron micrograph depicting a porosome (red arrow head) close to a microvilli (MV) at the apical plasma membrane (PM) of a pancreatic acinar cell. Note association of the porosome membrane (yellow arrow head) and the zymogen granule membrane (ZGM; red arrow head) of a docked zymogen granule (ZG), the membrane-bound secretory vesicle of exocrine pancreas. Also, a cross-section of the ring at the mouth of the porosome is seen (blue arrow head).

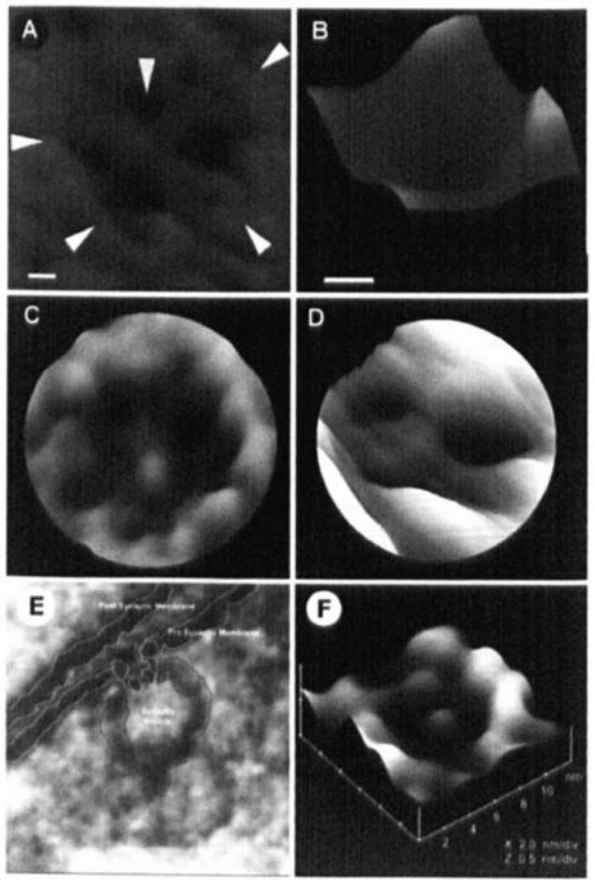

Figure 2. AFM micrograph of depressions, or porosomes, or fusion pores in live secretory cell of the exocrine pancreas (A, B), the growth hormone-secreting cell of the pituitary (C), in the chromaffin cell (D), and neurons (E, F). Note the pit (white arrow heads) with four depressions (yellow arrow head). A high-resolution AFM micrograph is shown in B. Bars = 40 nm for A and B. Similarly, AFM micrographs of porosomes in β-cell of the endocrine pancreas and mast cell have been observed. Electron micrograph of neuronal porosomes, which are 10–15-nm cup-shaped structures at the presynaptic membrane, where synaptic vesicles transiently dock and fuse to release vesicular contents (E). Atomic force micrograph of isolated neuronal porosome, reconstituted into lipid membrane (F).

biological samples at near-nanometer resolution, sample processing resulting in morphological alterations remained a major concern. Then, in the mid 1980s, scanning probe microscopy evolved (1, 28), further extending our perception of the living world to the near-atomic realm. One such scanning probe microscope, the AFM, has helped overcome both limitations of light and electron microscopy, enabling determination of the structure and dynamics of single biomolecules and live cells in three dimensions, at near-angstrom resolution. This unique capability of the AFM in combination with conventional tools and approaches has provided an understanding of cellular secretion (1–21) and membrane fusion (9, 17, 18, 29) at the molecular level.

The resolving power of the light microscope is dependent on the wavelength of the light used and, hence, 250–300 nm in lateral and much less in depth resolution can at best be achieved using light for imaging. The porosome or fusion pore in live secretory cells are cup-shaped structures measuring 100–180 nm at its opening and 15–35 nm in relative depth in the exocrine pancreas and just 10 nm at the presynaptic membrane of nerve terminals. As a result, it had evaded visual detection until its discovery using the AFM (3–8, 15). The development of the AFM (28) has enabled the imaging of live cells in physiological buffer at nanometer to subnanometer resolution. In AFM, a probe tip microfabricated from silicon or silicon nitride and mounted on a cantilever spring is used to scan the surface of the sample at a constant force. Either the probe or the sample can be precisely moved in a raster pattern using an *x-y-z* piezo tube to scan the surface of the sample. The deflection of the cantilever measured optically is used to generate an isoforce relief of the sample (30). Force is thus used by the AFM to image surface profiles of objects, such

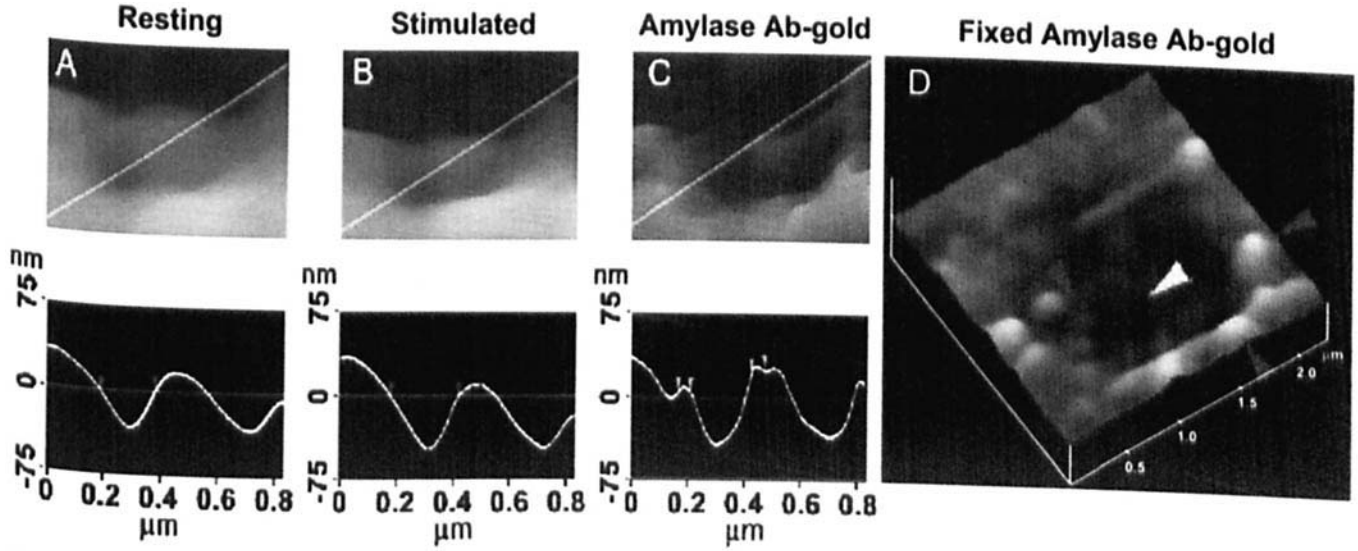

Figure 3. Depressions are fusion pores, or porosomes. Porosomes dilate to allow expulsion of vesicular contents. (A, B) AFM micrographs and section analysis of a pit and two out of the four fusion pores, or porosomes, demonstrating enlargement following stimulation of secretion. (C) Exposure of live cells to gold-conjugated amylase antibody (Ab) results in specific localization of immunogold to the porosome opening. Amylase is one of the proteins within secretory vesicles of the exocrine pancreas. (D) AFM micrograph of a fixed pancreatic acinar cell, demonstrating a pit and porosomes within, immunogold-labeling amylase at the site. Blue arrowheads point to immunogold clusters and the yellow arrowhead points to a porosome (4).

as live cells and subcellular structures, submerged in physiological buffer solutions, at ultrahigh resolution and in real time (3–8).

The Porosome

Earlier electrophysiological studies on mast cells suggested the existence of fusion pores at the cell plasma membrane (PM), which became continuous with the secretory vesicle membrane following stimulation of secretion (31). Studies on live secretory cells using the AFM revealed, for the first time, the physical existence of the fusion pore or porosome and determined its structure and dynamics in the exocrine pancreas (3, 4, 7, 8), in neuroendocrine cells (5, 6), and in neurons (15) at nanometer to subnanometer resolution and in real time.

Isolated live pancreatic acinar cells in physiological buffer, when imaged with the AFM (3, 4, 7, 8), reveal at the apical PM a group of circular pits measuring 0.4–1.2 µm in diameter, contain smaller depressions (Fig. 1). Each depression averages between 100 and 180 nm in diameter, and typically 3–4 depressions are located within a pit. The basolateral membrane of acinar cells is devoid of either pits or depressions. High-resolution AFM images of depressions in live cells further reveal a cone-shaped morphology. The depth of each depression cone measures 15–35 nm. Similarly, growth hormone (GH)-secreting cells of the pituitary gland, chromaffin cells, β-cells of the endocrine pancreas, mast cells, and neurons, all possess depressions at their PM, suggesting their universal presence in secretory cells. Exposure of pancreatic acinar cells to a secretagogue (mastoparan) results in a time-dependent increase (20%–35%) in depression diameter and relative depth, followed by a return to resting size on completion of secretion (3, 4, 7, 8). No demonstrable change in pit size is detected following stimulation of secretion (3). Enlargement of depression diameter and an increase in its relative depth after exposure to secretagogues correlate with increased secretion. Conversely, exposure of pancreatic acinar cells to cytochalasin B, a fungal toxin that inhibits actin polymerization and secretion, results in a 15%–20% decrease in depression size and a consequent 50%–60% loss in secretion (3). Results from these studies suggested depressions to be the fusion pores in pancreatic acinar cells. Furthermore, these studies demonstrate the involvement of actin in regulation of both the structure and function of depressions. Analogous to pancreatic acinar cells, examination of resting GH-secreting cells of the pituitary (5) and chromaffin cells of the adrenal medulla (6) also reveal the presence of pits and depressions at the cell PM (Fig. 2). The presence of porosomes in neurons, β-cells of the endocrine pancreas, and in mast cells have also been demonstrated (Fig. 2; Refs. 14, 15). Depressions in resting GH cells measure 154 ± 4.5 nm (mean ± SE) in diameter. Exposure of GH cells to a secretagogue results in a 40% increase in depression diameter (215 ± 4.6 nm; $P < 0.01$), with no appreciable change in pit size (5). The enlargement of depression diameter during secretion and its decrease accompanied by loss in secretion following exposure to actin depolymerizing agents (3) suggested depressions to be the fusion pores. However, a more direct determination that depressions are fusion pores was achieved using immuno-AFM studies (Fig. 3). AFM localization at depressions of gold-conjugated antibody to secretory proteins demonstrated secretion to occur through depressions (4, 5). The membrane-bound

secretory vesicles in exocrine pancreas, called zymogen granules (ZGs), contain the starch-digesting enzyme amylase. AFM micrographs demonstrated localization of amylase-specific antibodies tagged with colloidal gold at depressions following stimulation of secretion (Fig. 3; Ref. 4). These studies confirm depressions to be the fusion pores, or porosomes, in pancreatic acinar cells, where membrane-bound secretory vesicles dock and fuse to release their contents. Similarly, in somatotrophs of the pituitary, gold-tagged growth hormone-specific antibody is found to selectively localize at depressions following stimulation of secretion (5), again identifying depressions in GH cells as fusion pores, or porosomes. The porosome at the cytosolic side of the plasma membrane in the exocrine pancreas (7) and in neurons (15) has also been imaged at near-nanometer resolution in live tissue in buffer.

To determine the morphology of the porosome at the cytosolic compartment of the cell, pancreatic PM preparations were used. Isolated PM in buffer, when placed on freshly cleaved mica, tightly adhere to the mica surface, enabling imaging by AFM. The PM preparations reveal scattered circular disks measuring 0.5–1 μm in diameter, with inverted cup-shaped structures within (7). The inverted cups range in height from 10 to 15 nm. In a number of studies, AFM micrographs reveal ZGs ranging in size from 0.4 to 1 μm in diameter, found associated with one or more of the inverted cups. This suggested the circular disks to be pits and the inverted cups to be fusion pores or porosomes. To further confirm the cup-shaped structures to be porosomes, immuno-AFM studies were performed on them. Because ZGs dock and fuse at the PM to release vesicular contents, it was hypothesized that, if porosomes are these sites, then PM-associated t-SNAREs should localize at the base of porosomes. The t-SNARE protein SNAP-23 has been identified and implicated in secretion from pancreatic acinar cells (32). A polyclonal monospecific SNAP-23 antibody recognizing a single 23-kDa band on Westerns of pancreatic PM fraction was used in such immuno-AFM studies. When the SNAP-23-specific antibody was added to the PM preparation during imaging with the AFM, the antibody selectively localized to the base of the cup-shaped structure, that is, the tip of the inverted cup. These results demonstrate that the inverted cup-shaped structures in the isolated PM preparations are the porosomes observed from the cytosolic compartment of the cell (7, 8). Target membrane proteins, SNAP-25 and syntaxin (t-SNARE), and secretory vesicle-associated membrane protein (v-SNARE), are part of the conserved protein complex involved in fusion of opposing bilayers (9, 17, 18, 29). Because membrane-bound secretory vesicles dock and fuse at porosomes to release vesicular contents, it suggests that t-SNAREs associate at the porosome complex. It was therefore no surprise that the t-SNARE protein SNAP-23, implicated in secretion from pancreatic acinar cells, was located at the tip of the inverted cup (i.e., the base of the porosome), where secretory vesicles transiently dock and fuse.

The structure of the porosome was further determined using transmission electron microscopy (TEM; Figs. 1 and 2; Refs. 7, 8). TEM studies confirm the fusion pore to have a cup-shaped structure, with similar dimensions as determined from AFM measurement. Additionally, TEM micrographs reveal porosomes to possess a basket-like morphology, with three lateral and a number of vertically arranged ridges. A ring at the base of the complex is also identified (7). Because porosomes are found to be stable structures at the cell PM, it was hypothesized that, if ZGs were to fuse at the base of the structure, it would be possible to isolate ZG-associated porosomes. Indeed, TEM studies performed on isolated ZG preparations reveal porosomes associated with docked vesicles (7, 8). As observed in whole cells, vertical structures were found to originate from within the porosome complex and appear attached to its membrane. As discussed later in this review, studies using full-length recombinant SNARE proteins and artificial lipid membranes demonstrated that t- and v-SNAREs located in opposing bilayers interact in a circular array to form conducting pores (9). Similar circular structures observed at the base of the porosome and SNAP-23 immunoreactivity found to localize at this site, suggest that the t-SNAREs present at the base of porosomes are possibly arranged in a ring pattern.

Porosome: Isolation, Composition, and Reconstitution

In the last decade, a number of studies demonstrate the involvement of cytoskeletal proteins in secretion, and some studies implicate direct interaction of cytoskeleton protein with SNAREs (3, 33–37). Furthermore, actin and microtubule-based cytoskeleton have been implicated in intracellular vesicle traffic (3, 34). Fodrin, which was previously implicated in exocytosis (33), has recently been shown to directly interact with SNAREs (35). Studies demonstrate α-fodrin to regulate exocytosis via its interaction with t-SNARE syntaxin family of proteins (37). The c-terminal coiled coil region of syntaxin interacts with α-fodrin, a major component of the submembranous cytoskeleton. Similarly, vimentin filaments interact with SNAP23/25 and hence are able to control the availability of free SNAP23/25 for assembly of the SNARE complex (34). All these findings suggest that vimentin, α-fodrin, actin, and SNAREs may be part of the porosome complex. Additional proteins, such as v-SNARE (VAMP or synaptobrevin), synaptophysin, and myosin, may associate when the porosome establishes continuity with the secretory vesicle membrane. The globular tail domain of myosin V contains a binding site for VAMP, which is bound in a calcium-independent manner (36). Further interaction of myosin V with syntaxin requires both calcium and calmodulin. It has been suggested that VAMP acts as a myosin V receptor on secretory vesicles and regulates formation of the SNARE complex (36). Interaction of VAMP with synaptophysin and myosin V has also been observed (37). In agreement with

these earlier findings, recent studies demonstrate the association of SNAP-23, syntaxin 2, cytoskeletal proteins actin, α-fodrin, vimentin, and calcium channels β3 and α1c, together with the SNARE regulatory protein NSF, in porosomes (7, 8). Additionally, chloride ion channels ClC2 and ClC3 are identified as part of the porosome complex (7, 8). Isoforms of the various proteins identified in the porosome complex have also been demonstrated using 2D-BAC gel electrophoresis (8, 14). Three isoforms each of the calcium ion channel and vimentin have been found in porosomes (8). Using yeast two-hybrid analysis, recent studies confirm the presence and interaction of some of these proteins with t-SNAREs within the porosome complex (14).

The size and shape of the immunoisolated porosome complex was determined in greater detail when examined using both negative staining EM and by AFM (8). The images of the immunoisolated porosome obtained by both EM and AFM were superimposable (8). The immunoisolated supramolecular porosome complex has also been reconstituted into liposomes and in lipid bilayers (8). Transmission electron micrographs of porosome-reconstituted liposomes reveal a 150–200-nm cup-shaped, basket-like structure as observed of the porosome when coisolated with ZGs. To test the functionality of reconstituted porosome complexes, purified porosomes were reconstituted into lipid membranes in an electrophysiological bilayer setup (EPC9) and challenged with isolated ZGs (in reconstituted porosomes from exocrine pancreas) or synaptic vesicles (in reconstituted neuronal porosomes). Both the electrical activity of the reconstituted membrane and the transport of vesicular contents from the *cis* to the *trans* compartment were monitored. Results of these experiments demonstrate that the lipid membrane-reconstituted porosomes are functional supramolecular complexes (Fig. 4; Ref. 8). The ZGs fuse at the porosome-reconstituted bilayer, which is demonstrated by an increase in capacitance and conductance and a time-dependent release of the ZG enzyme amylase from *cis* to the *trans* compartment of the bilayer chamber (Fig. 4). Amylase is detected using immunoblot analysis of the buffer in the *cis* and *trans* compartment, using a previously characterized amylase-specific antibody (4). As observed in immunoblot assays of isolated porosomes, chloride channel activity is also detected in the reconstituted porosome complex, and the chloride channel inhibitor DIDS inhibits current activity in the reconstituted porosome. Similarly, the structure (Figs. 2 and 5) and biochemical composition of the neuronal porosome has also been determined (15). In summary, these studies demonstrate that the porosome in the exocrine pancreas and in neurons are 100–180 nm and 8–12 nm in diameter, respectively. The porosomes are supramolecular cup-shaped lipoprotein baskets at the cell PM, where membrane-bound secretory vesicles transiently dock and fuse to release vesicular contents to the outside.

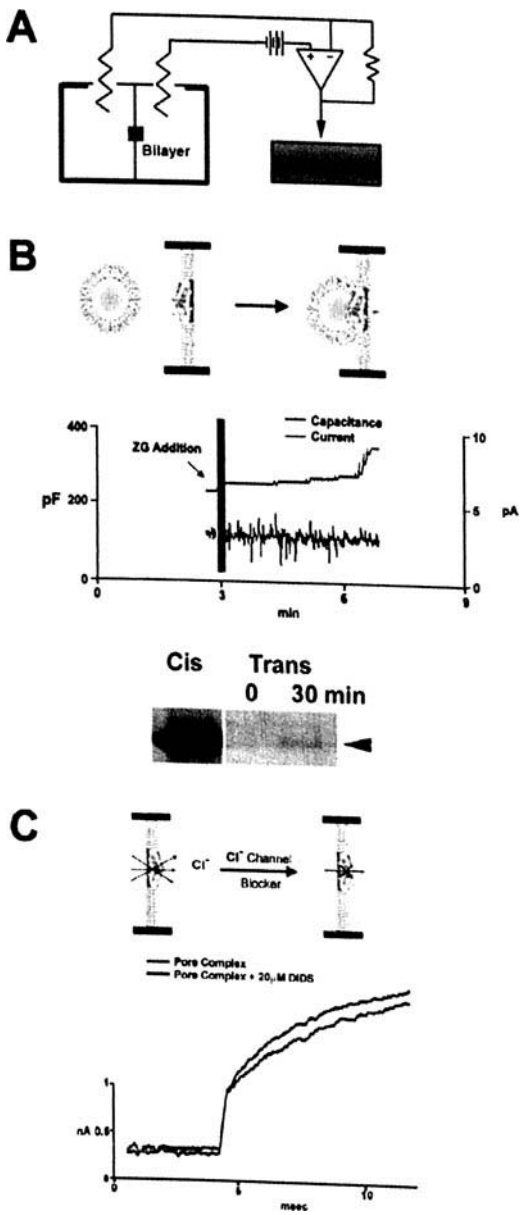

Figure 4. Lipid bilayer-reconstituted porosome complex is functional. (A) Schematic drawing of the bilayer setup for electrophysiological measurements. (B) Zymogen granules (ZGs) added to the *cis* side of the bilayer fuse with the reconstituted porosomes, as demonstrated by an increase in capacitance and current activities and a concomitant time-dependent release of amylase (a major ZG content) to the *trans* side of the membrane. The movement of amylase from the *cis* to the *trans* side of the chamber was determined by immunoblot analysis of the contents in the *cis* and the *trans* chamber over time. (C) As demonstrated by immunoblot analysis of the immunoisolated complex, electrical measurements in the presence and absence of chloride ion channel blocker DIDS demonstrate the presence of chloride channels in association with the complex.

Molecular Mechanism of Membrane Fusion

As briefly elucidated earlier in this article, membrane fusion is mediated via a specialized set of proteins at the secretory vesicle membrane and the cell plasma membrane. Three soluble N-ethylmaleimide-sensitive factor (NSF)-attachment protein receptors (SNAREs) have been impli-

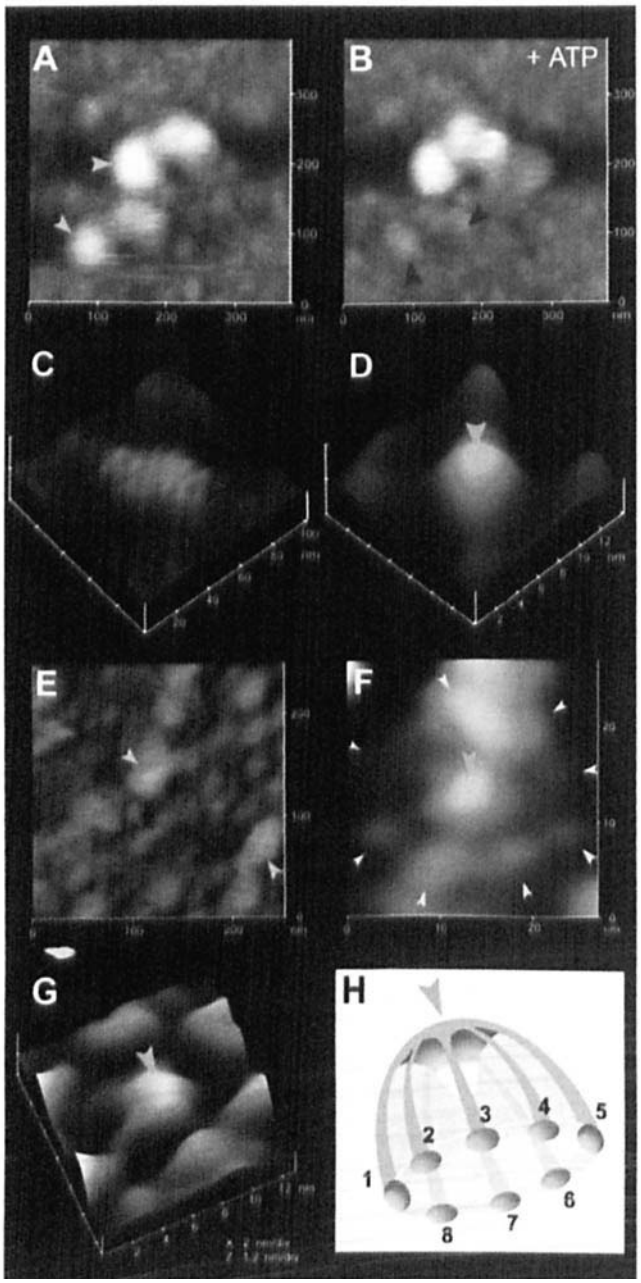

Figure 5. AFM micrographs revealing the dynamics of docked synaptic vesicles at porosomes and the porosome architecture in greater detail. (A) AFM micrograph of five docked synaptic vesicle at porosomes. (B) Addition of 50 μM ATP dislodges two synaptic vesicles at the lower left and exposes the porosome patches (red arrowheads). This also reveals that a single synaptic vesicle may dock at more than one porosome complex. (C–G) AFM micrographs obtained at higher imaging forces (300–500 pN rather than $<$200 pN) reveal porosomes architecture at greater detail. (C) AFM micrograph of one of the porosome patches where a synaptic vesicle was docked before ATP exposure. (D) Base of a single porosome. (E) High-force AFM micrograph of the cytosolic face of the presynaptic membrane, demonstrating the ribbon arrangement of porosome patches (red arrowhead) and docked synaptic vesicles (blue arrowheads). Note how the spherical synaptic vesicles are compressed and flattened at higher imaging forces. (F, G) At such higher imaging forces, porosomes reveal the presence of eight globular structures (yellow arrowhead) surrounding a central plug (green arrowhead), as demonstrated in the (H) schematic diagram.

cated in membrane fusion (29). Target membrane proteins, SNAP-25 and syntaxin (t-SNARE), and secretory vesicle-associated membrane protein (v-SNARE), are part of the conserved protein complex involved in fusion of opposing bilayers (29). The molecular mechanism of the involvement of SNAREs to bring about membrane fusion remained unknown until 2002 (9, 17, 18). The structure and arrangement of SNAREs, when associated with lipid bilayers, were first determined using the AFM (9). A bilayer electrophysiological assay allowed measurements of membrane conductance and capacitance before and after t-SNARE- or v-SNARE-reconstitution and following exposure to v-SNARE- or t-SNARE-reconstituted lipid vesicles. Results from these studies demonstrate that t-SNAREs and v-SNARE, when present in opposing bilayers, interact in a circular array, and, in the presence of calcium, form conducting pores (9). The interaction of t-/v-SNARE proteins to form a conducting pore or channel is strictly dependent on the presence of t-SNAREs and v-SNARE in opposing bilayers. Addition of purified recombinant v-SNARE to a t-SNARE-reconstituted lipid membrane increased only the size of the globular t-SNARE oligomer without influencing the electrical properties of the membrane (9). However, when t-SNARE vesicles are added to v-SNARE-reconstituted membrane, SNAREs assemble in a ring pattern (Fig. 6) and a stepwise increase in capacitance, and conductance is observed (9). Thus, t- and v-SNAREs are required to reside in opposing bilayers to allow appropriate t-/v-SNARE interactions leading to membrane fusion only in the presence of calcium (9). Studies using SNARE-reconstituted liposomes and bilayers (17) demonstrate (i) a slow fusion rate (τ = 16 min) between t- and v-SNARE-reconstituted liposomes in the absence of Ca^{2+}; and (ii) exposure of t-/v-SNARE liposomes to Ca^{2+} drives vesicle fusion on a near physiological-relevant time scale ($\tau \sim$ 10 sec), demonstrating an essential role of Ca^{2+} in membrane fusion. Because the Ca^{2+} effect on membrane fusion in SNARE-reconstituted liposomes is downstream of SNAREs, it suggests a regulatory role for Ca^{2+}-binding proteins in membrane fusion in the physiological state (17). It is further demonstrated from these studies that, in the physiological state in cells, both SNAREs and Ca^{2+} operate as the minimal fusion machinery (17). Native and synthetic vesicles exhibit a significant negative surface charge primarily due to the polar phosphate head groups. These polar head groups produce a repulsive force, preventing aggregation and fusion of apposing vesicles. SNAREs bring opposing bilayers closer, to within a distance of 2–3 Å (Fig. 7), allowing Ca^{2+} to bridge them (17). The bound Ca^{2+} then leads to the expulsion of water between the bilayers at the bridging site, allowing lipid mixing and membrane fusion. Hence, SNAREs, besides bringing apposing bilayers closer, dictate the site and size of the fusion area during secretion. The size of the t-/v-SNARE complex forming the pore is dictated by the curvature of the opposing membranes, hence depends on the size of t-/v-SNARE-reconstituted

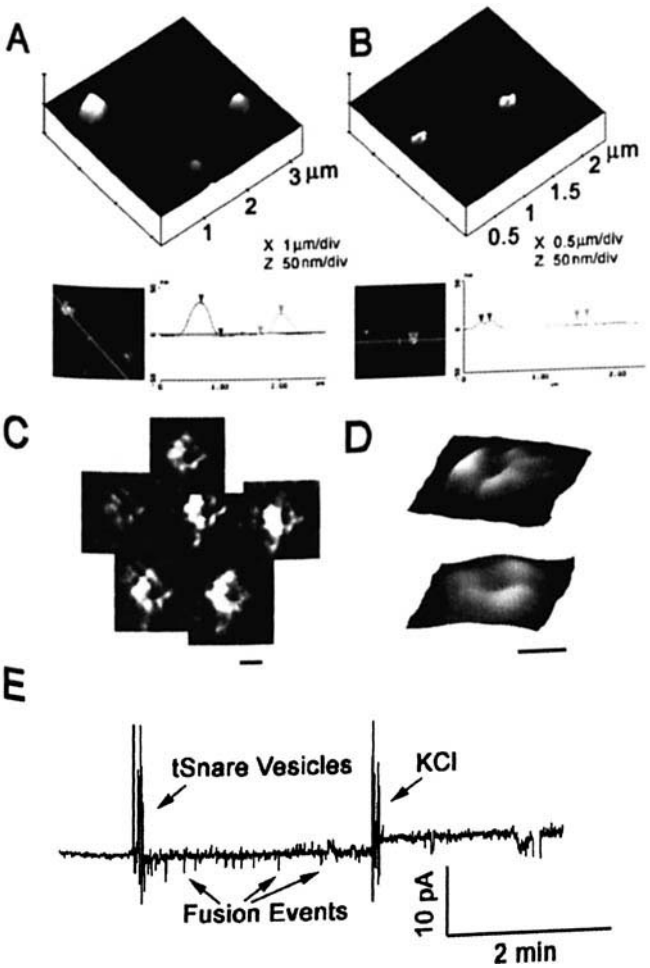

Figure 6. Pore-like structures are formed when t-SNAREs and v-SNARE in opposing bilayers interact. (A) Unfused v-SNARE vesicles on t-SNARE reconstituted lipid membrane. (B) Dislodgement or fusion of v-SNARE-reconstituted vesicles with a t-SNARE-reconstituted lipid membrane exhibit formation of pore-like structures due to the interaction of v- and t-SNAREs in a circular array. The size of the pores range between 50 and 150 nm (B–D). Several three-dimensional AFM-amplitude images of SNAREs arranged in a circular array (C) and some at higher resolution (D), illustrating a pore-like structure at the center. Scale bar is 100 nm. Recombinant t-SNAREs and v-SNARE in opposing bilayers drive membrane fusion. (E) When t-SNARE vesicles were exposed to v-SNARE reconstituted bilayers, vesicles fused. Vesicles containing nystatin/ergosterol and t-SNAREs were added to the *cis* side of the bilayer chamber. Fusion of t-SNARE-containing vesicles with the membrane observed as current spikes that collapse as the nystatin spreads into the bilayer membrane. To determine membrane stability, the transmembrane gradient of KCl was increased, allowing gradient-driven fusion of nystatin-associated vesicles.

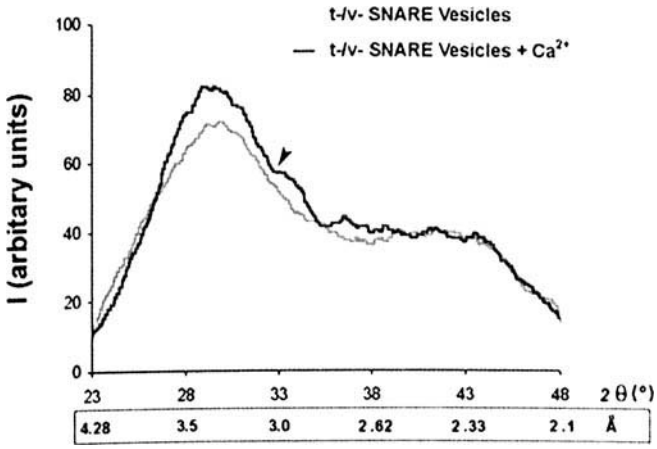

Figure 7. Wide-angle x-ray diffraction patterns of interacting SNARE vesicles. Representative diffraction profiles from one of four separate experiments using t- and v-SNARE-reconstituted lipid vesicles, both in the presence or absence of 5 m*M* Ca^{2+} are shown. Arrows mark appearance of a new peak in the x-ray diffractogram following addition of calcium.

vesicles. The smaller the vesicles, the smaller the pores formed (unpublished observation).

However, at the atomic level, how does Ca^{2+} bring about membrane fusion? This was resolved in a recent study (18). Calcium ion is essential for life processes and is found in every cell. Ca^{2+} participates in diverse cellular processes, such as metabolism, secretion, proliferation, muscle contraction, cell adhesion, learning, and memory. Although calcium is abundantly present within the cell, it is well sequestered and is available only on demand. Upon certain cellular stimulus for instance, Ca^{2+} concentration at specific locations (i.e., nanoenvironment) within the cell is elevated by several orders of magnitude within a brief period (some in <1 msec). This prompt mobilization of Ca^{2+} is essential for many physiological processes, such as the release of neurotransmitters or cell signaling. A unique set of chemical and physical properties of the Ca^{2+} ion make it ideal for performing these biochemical reactions. Calcium ion $[Ca^{2+}]$ exists in its hydrated state within cells. The properties of hydrated calcium have been extensively studied using x-ray diffraction and neutron scattering in combination with molecular dynamics simulations (38–41). The molecular dynamic simulations include three-body corrections compared with *ab initio* quantum mechanics/molecular mechanics molecular dynamics simulations. First principles molecular dynamics have also been used to investigate the structural, vibrational, and energetic properties of $[Ca(H_2O)_n]^{2+}$ clusters and the hydration shell of calcium ion. These studies demonstrate that hydrated calcium $[Ca(H_2O)_n]^{2+}$ has more than one shell around the Ca^{2+}, with the first hydration shell around the Ca^{2+} having six water molecules in an octahedral arrangement (39). In studies using light scattering and x-ray diffraction of SNARE-reconstituted liposomes, it was demonstrated that fusion proceeds only when Ca^{2+} ions are available between the t- and v-SNARE-apposed bilayers (Fig. 8; Ref. 18).

To monitor interaction(s) between Ca^{2+} ions and phosphate on the lipid membrane head groups, an x-ray diffraction method was used (17). This experimental approach for monitoring interbilayers contacts essentially requires the presence of (i) highly concentrated lipid suspensions (10 m*M* and above) favoring a multitude of intervesicular contacts; and (ii) a fully hydrated liposomes, where vesicles have full freedom to interact with each other in solution, hence establishing a confined hydrated area

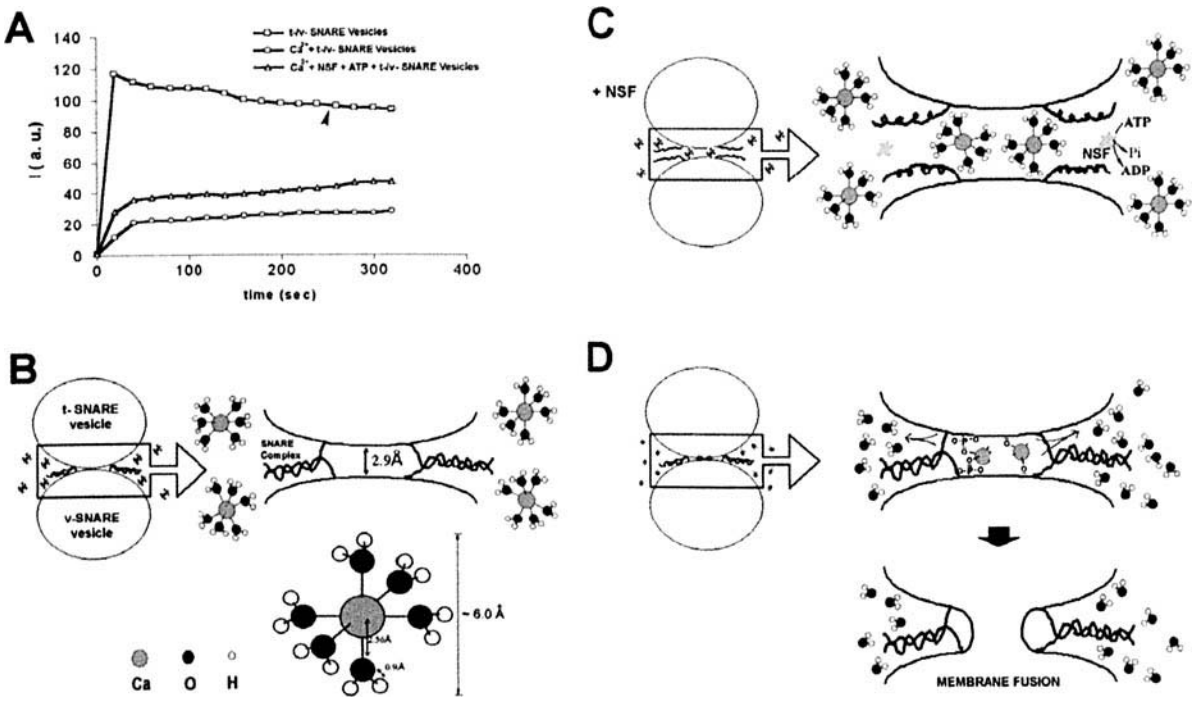

Figure 8. Light-scattering profiles of SNARE-associated vesicle interactions. (A, B) Addition of t-SNARE and v-SNARE vesicles in calcium-free buffer lead to a significant increase in light scattering. Subsequent addition of 5 m*M* Ca^{2+} (marked by arrowhead) does not have any significant effect on light scattering (□). (A, C) In the presence of NSF-ATP (1 μg/ml) in assay buffer containing 5m*M* Ca^{2+}, there was significantly inhibited vesicle aggregation and fusion (△). (A, D) When the assay buffer was supplemented with 5m*M* Ca^{2+} before addition of t- and v-SNARE vesicles, it led to a 4-fold decrease in light scattering intensity due to Ca^{2+}-induced aggregation and fusion of t-/v-SNARE apposed vesicles (○). Light-scattering profiles shown are representatives of four separate experiments.

between adjacent bilayers. This small fluid space could arise from interbilayer hydrogen-bond formation through water molecules (42) and additional bridging forces contributed by trans-SNARE complex formation (9, 17). If these two conditions are met, then liposomes diffract as shown (Fig. 8). Mixing of t- and v-SNARE liposomes in the absence of Ca^{2+} leads to a diffuse and asymmetric diffractogram (depicted by the gray trace; Fig. 7), a typical characteristic of short-range ordering in a liquid system. In contrast, mixing the t-SNARE and v-SNARE liposomes in the presence of Ca^{2+} leads to a more structured diffractogram (depicted by the black trace; Fig. 7) with an approximately 12% increase in x-ray scattering intensity, pointing to an increase in the number of contacts between apposing bilayers established presumably by calcium-PO bridges, as previously suggested (43). The ordering effect of Ca^{2+} on interbilayer contacts observed in x-ray studies (18) is in good agreement with recent light microscopy, AFM, and spectroscopic studies suggesting close apposition of PO lipid head groups in the presence of Ca^{2+} ions followed by formation of Ca^{2+}-PO bridges between adjacent bilayers (17, 44). An x-ray study shows that the effect of Ca^{2+} on bilayer orientation and interbilayer contacts is most prominent in the area of 3 Å, with additional appearance of a new peak (shoulder) at 2.8 Å (depicted by the arrow; Fig. 7), both of which are within the ionic radius of Ca^{2+} (18). These studies suggest that the ionic radius of Ca^{2+} may play an important role in membrane fusion. But there remained a major spatial problem, which was recently resolved (18). As discussed earlier, calcium ions [Ca^{2+}] exist in their hydrated state within cells. Hydrated calcium $[Ca(H_2O)_n]^{2+}$ has more than one shell around the Ca^{2+}, with the first hydration shell having six water molecules in an octahedral arrangement (38), measuring ~6 Å (Fig. 8). Studies reveal that for hydrated Ca^{2+} ion, depending on its coordination number, the nearest average neighbor Ca^{2+}-O and Ca^{2+}-H distances are at r ~ 2.54 Å and r ~ 3.2 Å, respectively, in the first hydration shell. How then would a hydrated calcium ion measuring ~6 Å fit between the 2.8–3 Å space established by t-/v-SNAREs, between the apposing bilayers? One possibility would be that calcium has to be present in the buffer solution when t-SNARE vesicles and v-SNARE vesicles meet. If t- and v-SNARE vesicles are allowed to mix in a calcium-free buffer, no fusion should occur. This was tested in a published study (18). Light-scattering experiments (Fig. 8) were performed on t-SNARE- and v-SNARE-reconstituted phospholipids vesicles in the presence and absence of calcium and in the presence of NSF+ATP. NSF or N-ethylmaleimide-sensitive factor is an ATPase that is known to disassemble the t-/v-SNARE complex. Using the light-scattering measurements, aggregation and membrane fusion of lipid vesicles can be monitored on the second time scale (17, 45). The initial rapid increase in intensity of light scattering was initiated by the addition of t- and v-SNARE vesicles into the cuvette, followed by a slow decay of light scattering (Fig. 8),

representing interactions between vesicles in solution. These studies show that, if t-SNARE vesicles and v-SNARE vesicles are allowed to interact before calcium addition (depicted by arrow; Fig. 8), no significant change in light scattering is observed (there is no significant decrease in scattering, attributed to little fusion between the vesicle suspension). On the contrary, when calcium is present in the buffer solution before addition of the t-SNARE and v-SNARE vesicles, there is a marked drop in light scattering, as a result of vesicle aggregation and fusion (Fig. 8). However, in the presence of NSF-ATP in the assay buffer containing calcium, a significant inhibition in aggregation and fusion of proteoliposomes is observed (Fig. 8). NSF, in the absence of ATP, has no effect on the light-scattering properties of the vesicle mixture. These results demonstrate that NSF-ATP disassembles the SNARE complex, thereby reducing the number of interacting vesicles in solution. In addition, disassembly of trans-SNARE complex will then leave apposed bilayers widely separated, out of reach for the formation of Ca^{2+}-PO bridges (Fig. 8). Similarly, if the restricted area between adjacent bilayers deliniated by the circular arrangement of the t-/v-SNARE complex (9) is preformed, then hydrated Ca^{2+} ions are too large (Fig. 8) to be accommodated between bilayers and, hence, subsequent addition of Ca^{2+} would have no effect (Fig. 8). However, when t-SNARE vesicles interact with v-SNARE vesicles in the presence of Ca^{2+}, the t-/v-SNARE complex formed allows formation of calcium-phosphate bridges between opposing bilayers, leading to the expulsion of water around the Ca^{2+} ion to enable lipid mixing and membrane fusion (Fig. 8). Thus, x-ray and light-scattering studies (18) demonstrate that calcium bridging of the apposing bilayers is required to enable membrane fusion. This calcium bridging of apposing bilayers leads to the release or expulsion of water from the hydrated Ca^{2+} ion, leading to bilayer destabilization and membrane fusion. It could also be argued that the binding of calcium to the phosphate head groups of the apposing bilayers may displace the loosely coordinated water at the PO groups, further adding to the destabilization of the lipid bilayer, leading to membrane fusion.

The Regulated Expulsion of Intravesicular Contents During Secretion

Once the membrane-bound secretory vesicle fuses at the base of porosomes, establishing continuity between the two compartments, how is the vesicle content expelled? Studies reveal that vesicle swelling is required for the expulsion of intravesicular contents during secretion (46). It has been demonstrated (46) that the extent of vesicle swelling is directly proportional to the amount of intravesicular contents expelled, hence, providing cells with the ability to further regulate the amount of release of secretory products. Direct observations of the requirement of secretory vesicle swelling in secretion (46) provides, for the first time, an understanding of the appearance of empty and partially empty vesicles following secretion (10, 26, 47).

Electron micrograph of pancreatic acinar cells and isolated live pancreatic acinar cells in near physiological buffer, when imaged using AFM at high force (200–300 pN), reveal the profile of the secretory vesicles called zymogen granules (ZGs), lying immediately under the apical plasma membrane of the cells. Within 2.5 mins of exposure to a physiological secretory stimulus (1 μM carbamylcholine), the majority of ZGs within cells swell, followed by a decrease in ZG size, by which time most of the release of secretory products from within ZGs had occurred. These studies (46) reveal, for the first time in live cells, intracellular swelling of secretory vesicles following stimulation of secretion and their deflation following partial discharge of vesicular contents. Measurements of intracellular ZG size further revealed that different vesicles swell differently following a secretory stimulus. This differential swelling among ZGs within the same cell may explain why, following stimulation of secretion, some intracellular ZGs demonstrate the presence of less vesicular content than others following secretion, because they have discharged more of their contents due to greater swelling (10).

To determine precisely the role of swelling in the expulsion of intravesicular contents, the electrophysiological ZG-reconstituted lipid bilayer fusion assay (17), as described earlier, has been employed (46). The ZGs used in the bilayer fusion assays were characterized for their purity and their ability to respond to a swelling stimulus. As previously reported (19–21), exposure of isolated ZGs (Fig. 9A and B) to GTP resulted in ZG swelling (Fig. 9C; Ref. 46). Once again, similar to what is observed in live acinar cells, each isolated ZG responded differently to the same swelling stimulus. For example, the red arrowhead points to a ZG of which the diameter increased by 29% as opposed to the green arrowhead pointing to a ZG that increased only by a modest 8%. The differential response of isolated ZGs to GTP was further assessed by measuring changes in the volume of isolated ZGs of different sizes (Fig. 9D). The ZGs in the exocrine pancreas range in size from 0.2 to 1.3 μm in diameter (19). Not all ZGs swell following a GTP challenge. The volume of most ZGs increases between 5% and 20%. However, larger increases, up to 45%, are observed only in vesicles ranging from 250 to 750 nm in diameter (Fig. 9D). These studies demonstrate that, following stimulation of secretion, ZGs within pancreatic acinar cells swell, followed by a release of intravesicular contents through porosomes (7, 8) at the cell plasma membrane and a return to resting size on completion of secretion. On the contrary, isolated ZGs stay swollen following exposure to GTP because there is no outlet for release of the intravesicular contents. In acinar cells, little or no secretion is detected 2.5 mins following stimulation of secretion, although the ZGs within them have swelled. However, 5 mins following stimulation, ZGs deflated and the intravesicular α-amylase released from the acinar cell is

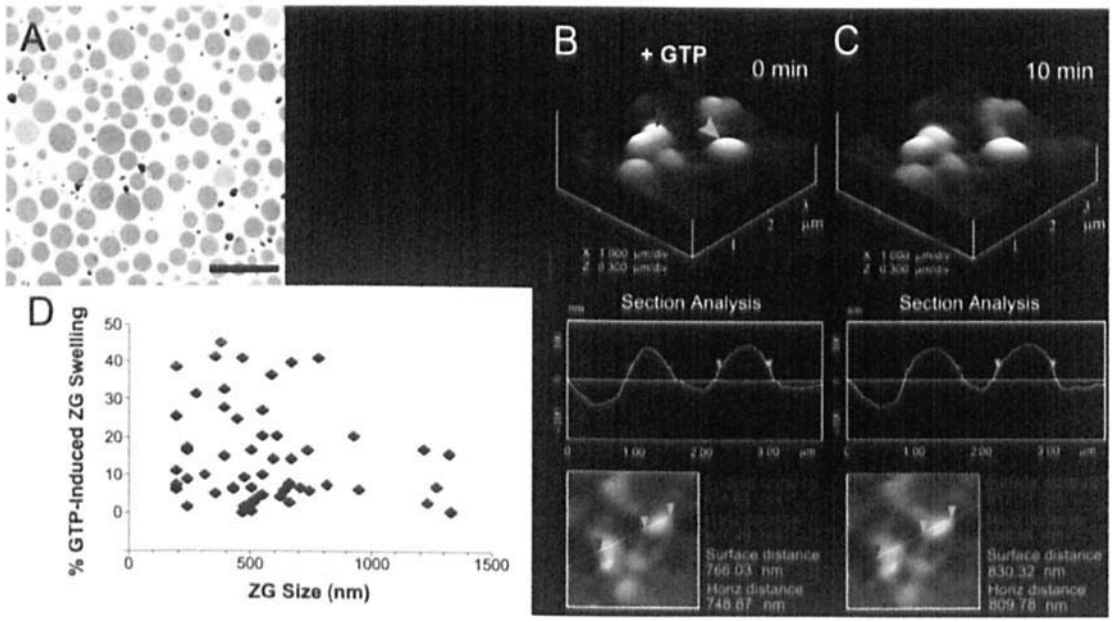

Figure 9. Swelling of isolated ZGs. (A) Electron micrograph of isolated ZGs demonstrating a homogeneous preparation. Bar = 2.5 μm. (B, C) Isolated ZGs, on exposure to 20 μ*M* GTP, swell rapidly. Note the enlargement of ZGs as determined by AFM-section analysis of two vesicles (red and green arrowheads). (D) Percentage ZG volume increase in response to 20 μ*M* GTP. Note how different ZGs respond to the GTP-induced swelling differently (46).

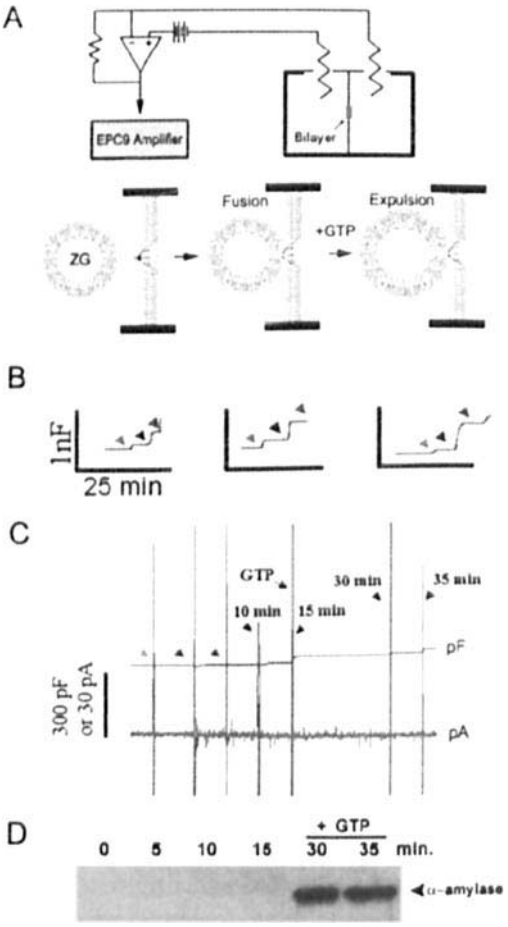

detectable, suggesting the involvement of ZG swelling in secretion.

In the electrophysiological bilayer fusion assay, immunoisolated fusion pores or porosomes from the exocrine pancreas were isolated and functionally reconstituted (8) into the lipid membrane of the bilayer apparatus and membrane conductance and capacitance continually monitored (Fig. 10A). Reconstitution of the porosome into the lipid membrane results in a small increase in capacitance (Fig. 10B), possibly due to the increase in membrane surface area contributed by incorporation of porosomes, ranging in size from 100 to 150 nm in diameter (8). Isolated

←

Figure 10. Fusion of isolated ZGs at porosome-reconstituted bilayer and GTP-induced expulsion of α-amylase. (A) Schematic diagram of the EPC9 bilayer apparatus showing the *cis* and *trans* chambers. Isolated ZGs, when added to the *cis* chamber, fuse at the bilayers-reconstituted porosome. Addition of GTP to the *cis* chamber induces ZG swelling and expulsion of its contents, such as α-amylase to the *trans* bilayers chamber. (B) Capacitance traces of the lipid bilayer from three separate experiments following reconstitution of porosomes (green arrowhead), addition of ZGs to the *cis* chamber (blue arrowhead), and the red arrowhead represents the 5-min time point after ZG addition. Note the small increase in membrane capacitance following porosome reconstitution and a greater increase when ZGs fuse at the bilayers. (C) In a separate experiment, 15 mins after addition of ZGs to the *cis* chamber, 20 μ*M* GTP was introduced. Note the increase in capacitance, demonstrating potentiation of ZG fusion. Flickers in current trace represent current activity. (D) Immunoblot analysis of α-amylase in the *trans* chamber fluid at different times following exposure to ZGs and GTP. Note the undetectable levels of α-amylase even up to 15 mins following ZG fusion at the bilayer. However, following exposure to GTP, significant amounts of α-amylase from within ZGs were expelled into the *trans* bilayers chamber (n = 6; Ref. 46).

ZGs, when added to the *cis* compartment of the bilayer chamber, fuse at the porosome-reconstituted lipid membrane (Fig. 10A), which is detected as a step increase in membrane capacitance (Fig. 10B). However, even after 15 mins of ZG addition to the *cis* compartment of the bilayer chamber, little or no release of the intravesicular enzyme α-amylase is detected in the *trans* compartment of the chamber (Fig. 10C and D). On the contrary, exposure of ZGs to 20 μ*M* GTP induces swelling (19–21) and results both in the potentiation of fusion as well as a robust expulsion of α-amylase into the *trans* compartment of the bilayer chamber (Fig. 10C and D). These studies demonstrated that, during secretion, secretory vesicle swelling is required for the efficient expulsion of intravesicular contents.

Within minutes or even seconds following stimulation of secretion, empty and partially empty secretory vesicles accumulate within cells. There may be two possible explanations for such accumulation of partially empty vesicles. Following fusion at the porosome, secretory vesicles may either remain fused for a brief period and therefore time would be the limiting factor for partial expulsion. An alternate scenario would be that secretory vesicles may not swell enough and therefore are unable to generate the required intravesicular pressure for complete discharge. Results from published studies (Fig. 10) suggest that it would be highly unlikely that generation of partially empty vesicles would result from brief periods of vesicle fusion at porosomes. Because, after addition of ZGs to the *cis* compartment of the bilayer apparatus, membrane capacitance continues to increase, although little or no detectable secretion occurred even after 15 mins (Fig. 10), it is suggested that either variable degrees of vesicle swelling or repetitive cycles of fusion and swelling of the same vesicle, or both, may operate during the secretory process. Under these circumstances, empty and partially empty vesicles could be generated within cells following secretion. To test this hypothesis, two key parameters have been examined (46). One is whether the extent of swelling is the same for all ZGs exposed to a certain concentration of GTP. The second is whether ZG is capable of swelling to different degrees. And if so, whether there is a correlation between extent of swelling and the quantity of intravesicular contents expelled. The answer to the first question is clear, that different ZGs respond to the same stimulus differently. Studies (46) reveal that different ZGs within cells, or in isolation, undergo different degrees of swelling, even though they are exposed to the same stimulus (carbamylcholine for live pancreatic acinar cells or GTP for isolated ZGs). The requirement of ZG swelling for expulsion of vesicular contents is further confirmed, when GTP dose dependently increased ZG swelling is translated into increased secretion of α-amylase (46). Although higher GTP concentrations elicited an increased ZG swelling, the extent of swelling between ZGs once again varied.

To determine if a similar or an alternate mechanism is responsible for the release of secretory products in a fast secretory cell, such as neurons, synaptosomes and synaptic vesicle preparation from rat brain has been studied (46). Because synaptic vesicle membrane is known to possess both Gi and Go proteins, it was hypothesized that GTP and Gi-agonist (mastoparan) would mediate vesicle swelling. To test this hypothesis, isolated synaptosomes were lysed to obtain synaptic vesicles and synaptosomal membrane. Isolated synaptosomal membrane, when placed on mica and imaged by the AFM in near-physiological buffer, reveal on the cytosolic side the presence of 40–50-nm diameter synaptic vesicles still docked to the presynaptic membrane. Similar to the ZGs, exposure of synaptic vesicles to 20 μ*M* GTP results in an increase in synaptic vesicle swelling. However, exposure to Ca^{2+} results in the transient fusion of synaptic vesicles at the presynaptic membrane, expulsion of intravesicular contents, and a consequent decrease in size of the synaptic vesicle. Additionally, as observed in ZGs of the exocrine pancreas, not all synaptic vesicles swell and, if they do, they swell to different degrees even though they had been exposed to the same stimulus. This differential response of synaptic vesicles within the same nerve terminal may dictate and regulate the potency and efficacy of neurotransmitter release. To further confirm synaptic vesicle swelling and determine the swelling rate, light-scattering experiments to monitor vesicle size have also been performed (46). Light-scattering studies demonstrate a mastoparan-dose-dependent increase in synaptic vesicle swelling. Mastoparan (20 μ*M*) induced a time-dependent (in seconds) increase of synaptic vesicle swelling, as opposed to the control peptide (Mast-17).

These studies (46) demonstrate that, following stimulation of secretion, ZGs, the membrane-bound secretory vesicles, in exocrine pancreas swell. Different ZGs swell differently, and the extent of their swelling dictates the amount of intravesicular contents to be expelled. ZG swelling is therefore a requirement for the expulsion of vesicular contents in the exocrine pancreas. Similar to ZGs, synaptic vesicle swelling enables the expulsion of neurotransmitters at the nerve terminal. This mechanism of vesicular expulsion during cell secretion may explain why partially empty vesicles are observed in secretory cells following secretion. The presence of empty secretory vesicles could result from multiple rounds of fusion-swelling-expulsion a vesicle may undergo during the secretory process. These results reflect the precise and regulated nature of cell secretion from the exocrine pancreas to neurons.

What is the molecular mechanism of secretory vesicle swelling? This has been addressed in studies using isolated ZGs (19–21). Isolated ZGs from exocrine pancreas swell rapidly in response to GTP (19). These studies suggested the involvement of rapid water gating into ZGs following exposure to GTP. Therefore, when the possible involvement of water channels, or aquaporins, in ZG swelling was explored (20), results from the study demonstrate the presence of aquaporin-1 (AQP1) at the ZG membrane and

its participation in GTP-mediated vesicle water entry and swelling (20). To further understand the molecular mechanism of secretory vesicle swelling, the regulation of AQP1 in ZGs has been determined (21). Detergent-solubilized ZGs immunoprecipitated with monoclonal AQP-1 antibody, coisolates AQP1, PLA2, $G_{\alpha i3}$, potassium channel IRK-8, and the chloride channel ClC-2 (21). Exposure of ZGs to either the potassium channel blocker glyburide or the PLA2 inhibitor ONO-RS-082 blocked GTP-induced ZG swelling. Red blood cells, known to possess AQP1 at the plasma membrane, also swell on exposure to the $G_{\alpha i}$-agonist mastoparan and respond similarly to ONO-RS-082 and glyburide as do ZGs (21). Additionally, liposomes reconstituted with the AQP-1 immunoisolated complex from solubilized ZGs were found to swell in response to GTP. Glyburide or ONO-RS-082 abolished the GTP effect in reconstituted liposomes. Furthermore, immunoisolate-reconstituted planar lipid membrane demonstrate conductance, which is sensitive to glyburide and an AQP1 specific antibody. These results demonstrate a $G_{\alpha i3}$-PLA2-mediated pathway and potassium channel involvement in AQP-1 regulation (21), contributing to our understanding of the molecular mechanism of ZG swelling.

Molecular Understanding of Cell Secretion

Fusion pores, or porosomes, are present in all secretory cells examined. From exocrine, endocrine, neuroendocrine cells, to neurons, where membrane-bound secretory vesicles dock and transiently fuse to expel vesicular contents. Porosomes in pancreatic acinar or GH-secreting cells are cup-shaped structures at the plasma membrane, with a 100–150-nm-diameter opening. Membrane-bound secretory vesicles ranging in size from 0.2 to 1.3 μm in diameter dock and fuse at porosomes to release vesicular contents. Following fusion of secretory vesicles at porosomes, only a 20%–35% increase in porosome diameter is demonstrated. It is therefore reasonable to conclude that secretory vesicles transiently dock and fuse at the site. In contrast with accepted belief, if secretory vesicles were to completely incorporate at porosomes, the PM structure would distend much wider than what is observed. Furthermore, if secretory vesicles were to completely fuse at the plasma membrane, there would be a loss in vesicle number following secretion. Examination of secretory vesicles within cells before and after secretion demonstrates that the total number of secretory vesicles remains unchanged following secretion (10, 26). However, the number of empty and partially empty vesicles increases significantly, supporting the occurrence of transient fusion of secretory vesicles at the porosome. Earlier studies in mast cells also demonstrated an increase in the number of spent and partially spent vesicles following stimulation of secretion, without any demonstrable increase in cell size. Similarly, secretory granules are recaptured largely intact after stimulated exocytosis in cultured endocrine cells (22). Other supporting evidence favoring transient fusion is the presence of neurotransmitter transporters at the synaptic vesicle membrane. These vesicle-associated transporters would be of little use if vesicles were to fuse completely at the plasma membrane to be compensatorily endocytosed at a later time. In further support, a recent study reports that single synaptic vesicles fuse transiently and successively without loss of vesicle identity (23). Although the fusion of secretory vesicles at the cell plasma membrane occurs transiently, complete incorporation of membrane at the cell plasma membrane would occur when cells need to incorporate signaling molecules, like receptors, second messengers, or ion channels, at the cell plasma membrane. The discovery of the porosome and an understanding of the molecular mechanism of membrane fusion and the swelling of secretory vesicles required for expulsion of vesicular contents provide an understanding of secretion and membrane fusion in cells at the molecular level. These findings have prompted many laboratories to work in the area and further confirm these findings. Thus, the porosome is a supramolecular structure universally present in secretory cells, from the exocrine pancreas to the neurons, and in the endocrine to neuroendocrine cells, where membrane-bound secretory vesicles transiently dock and fuse to expel vesicular contents. Hence, the secretory process in cells is highly regulated and is orchestrated by a number of ions and biomolecules.

I thank Won Jin Cho for the preparation of the manuscript.

1. Hörber JKH, Miles MJ. Scanning probe evolution in biology. Science 302:1002–1005, 2003.
2. Anderson LL. Discovery of a new cellular structure-the porosome: elucidation of the molecular mechanism of secretion. Cell Biol Int 28:3–5, 2004.
3. Schneider SW, Sritharan KC, Geibel JP, Oberleithner H, Jena BP. Surface dynamics in living acinar cells imaged by atomic force microscopy: identification of plasma pembrane structures involved in exocytosis. Proc Natl Acad Sci U S A 94:316–321, 1997.
4. Cho SJ, Quinn AS, Stromer MH, Dash S, Cho J, Taatjes DJ, Jena BP. Structure and dynamics of the fusion pore in live cells. Cell Biol Int 26:35-42, 2002.
5. Cho SJ, Jeftinija K, Glavaski A, Jeftinija S, Jena BP, Anderson LL. Structure and dynamics of the fusion pores in live GH-secreting cells revealed using atomic force microscopy. Endocrinology 143:1144–1148, 2002.
6. Cho SJ, Wakade A, Pappas GD, Jena BP. New structure involved in transient membrane fusion and exocytosis. Ann N Y Acad Sci 971:254–256, 2002.
7. Jena BP, Cho SJ, Jeremic A, Stromer MH, Abu-Hamdah R. Structure and composition of the fusion pore. Biophys J 84:1337–1343, 2003.
8. Jeremic A, Kelly M, Cho SJ, Stromer MH, Jena BP. Reconstituted fusion pore. Biophys J 85:2035–2043, 2003.
9. Cho SJ, Kelly M, Rognlien KT, Cho J, Hoerber JKH, Jena BP. SNAREs in opposing bilayers interact in a circular array to form conducting pores. Biophys J 83:2522–2527, 2002.
10. Cho SJ, Cho J, Jena BP. The number of secretory vesicles remains unchanged following exocytosis. Cell Biol Int 26:29–33, 2002.
11. Jena BP. Fusion pore in live cells. NIPS 17:219–222, 2002.

12. Jena BP. Fusion pore: structure and dynamics. J Endo. 176:169–174, 2003.
13. Jena BP. Exocytotic fusion: total or transient. Cell Biol Int 21:257–259, 1997.
14. Jena BP. Discovery of the porosome: revealing the molecular mechanism of secretion and membrane fusion in cells. J Cell Mol Med 8:1–21, 2004.
15. Cho WJ, Jeremic A, Rognlien KT, Zhvania MG, Lazrishvili I, Tamar B, Jena BP. Structure, isolation, composition and reconstitution of the neuronal fusion pore. Cell Biol Int 28:699–708, 2004.
16. Kelly M, Cho WJ, Jeremic A, Abu-Hamdah R, Jena BP. Vesicle swelling regulates content expulsion during secretion. Cell Biol Int 28:709–716, 2004.
17. Jeremic A, Kelly M, Cho WJ, Cho SJ, Horber JKH, Jena BP. Calcium drives fusion of SNARE-apposed bilayers. Cell Biol Int 28:19–31, 2004.
18. Jeremic A, Cho WJ, Jena BP. Membrane fusion: what may transpire at the atomic level. J Biol Phys Chem 4:139–142, 2004.
19. Jena BP, Schneider SW, Geibel JP, Webster P, Oberleithner H, Sritharan KC. G_i regulation of secretory vesicle swelling examined by atomic force microscopy. Proc Natl Acad Sci U S A 94:13317–13322, 1997.
20. Cho SJ, Sattar AK, Jeong EH, Satchi M, Cho JA, Dash S, Mayes MS, Stromer MH, Jena BP. Aquaporin 1 regulates GTP-induced rapid gating of water in secretory vesicles. Proc Natl Acad Sci U S A 99:4720–4724, 2002.
21. Abu-Hamdah R, Cho WJ, Cho SJ, Jeremic A, Kelly M, Ilie AE, Jena BP. Regulation of the water channel aquaporin-1: isolation and reconstitution of the regulatory complex. Cell Biol Int 28:7–17, 2004.
22. Taraska JW, Perrais D, Ohara-Imaizumi M., Nagamatsu S, Almers W. Secretory granules are recaptured largely intact after stimulated exocytosis in cultured endocrine cells. Proc Natl Acad Sci U S A 100:2070–2075, 2003.
23. Aravanis AM, Pyle JL, Tsien RW. Single synaptic vesicles fusing transiently and successively without loss of identity. Nature 423:643–647, 2003.
24. Tojima T, Yamane Y, Takagi H, Takeshita T, Sugiyama T, Haga H, Kawabata K, Ushiki T, Abe K, Yoshioka T, Ito E. Three-dimensional characterization of interior structures of exocytotic apertures of nerve cells using atomic force microscopy. Neuroscience 101:471–481, 2000.
25. Thorn P, Fogarty KE, Parker I. Zymogen granule exocytosis is characterized by long fusion pore openings and preservation of vesicle lipid identity. Proc Natl Acad Sci U S A 101:6774–6779, 2004.
26. Lee JS, Mayes MS, Stromer MH, Scanes CG, Jeftinija S, Anderson LL. Number of secretory vesicles in growth hormone cells of the pituitary remains unchanged after secretion. Exp Biol Med 229:291–302, 2004.
27. Fix M, Melia TJ, Jaiswal JK, Rappoport JZ, You D, Söllner TH, Rothman JE, Simon SM. Imaging single membrane fusion events mediated by SNARE proteins. Proc Natl Acad Sci U S A 101:7311–7316, 2004.
28. Binnig G, Quate CF, Gerber CH. Atomic force microscope. Phys Rev Lett 56:930–933, 1986.
29. Weber T, Zemelman BV, McNew JA, Westerman B, Gmachi M, Parlati F, Söllner TH, Rothman JE. SNARE pins: minimal machinery for membrane fusion. Cell 92:759–772, 1998.
30. Alexander S, Hellemans L, Marti O, Schneir J, Elings V, Hansma PK. An atomic resolution atomic force microscope implemented using an optical lever. J Appl Physiol 65:164–167, 1989.
31. Monck JR, Oberhauser AF, Fernandez JM. The exocytotic fusion pore interface: a model of the site of neurotransmitter release. Mol Memb Biol 12:151–156, 1995.
32. Gaisano HY, Sheu L, Wong PP, Klip A, Trimble WS. SNAP-23 is located in the basolateral plasma membrane of rat pancreatic acinar cells. FEBS Lett 414:298–302, 1997.
33. Bennett V. Spectrin-based membrane skeleton: a multipotential adaptor between plasma membrane and cytoplasm. Physiol Rev 70:1029–1065, 1990.
34. Faigle W, Colucci-Guyon E, Louvard D, Amigorena S, Galli T. Vimentin filaments in fibroblasts are a reservoir for SNAP-23, a component of the membrane fusion machinery. Mol Biol Cell 11:3485–3494, 2000.
35. Goodson HV, Valetti C, Kreis TE. Motors and membrane traffic. Curr Opin Cell Biol 9:18–28, 1997.
36. Nakano M, Nogami S, Sato S, Terano A, Shirataki H. Interaction of syntaxin with α-fodrin, a major component of the submembranous cytoskeleton. Biochem Biophys Res Commun 288:468–475, 2001.
37. Ohyama A, Komiya Y, Igarashi M. Globular tail of myosin-V is bound to vamp/synaptobrevin. Biochem Biophys Res Commun 280:988–991, 2001.
38. Chialvo AA, Simonson JM. The structure of $CaCl_2$ aqueous solutions over a wide range of concentration. Interpretation of diffraction experiments via molecular simulation. J Chem Phys 119:8052–8061, 2003.
39. Bako I, Hutter J, Palinkas G. Car-Parrinello molecular dynamics simulation of the hydrated calcium ion. J Chem Phys 117:9838–9843, 2002.
40. Schwenk CF, Loeffler HH, Rode BM. Molecular dynamics simulations of Ca^{2+} in water: comparison of a classical simulation including three-body corrections and Born-Oppenheimer *ab initio* and density functional theory quantum mechanical/molecular mechanics simulations. J Chem Phys 115:10808–10813, 2001.
41. Licheri G, Piccaluga G, Pinna G. X-ray diffraction study of the average solute species in $CaCl_2$ aqueous solutions. J Chem Phys 64:2437–2446, 1976.
42. McIntosh TJ. Short-range interactions between lipid bilayers measured by X-ray diffraction. Curr Opin Struct Biol 10:481–485, 2000.
43. Portis A, Newton C, Pangborn W, Papahadjopoulos D. Studies on the mechanism of membrane fusion: evidence for an intermembrane Ca^{2+}-phospholipid complex, synergism with Mg^{2+}, and inhibition by spectrin. Biochemistry 18:780–790, 1979.
44. Laroche G, Dufourc EJ, Dufoureq J, Pezolet M. Structure and dynamics of dimyristoylphosphatidic acid/calcium complex by 2H NMR, infrared, spectroscopies and small-angle x-ray diffraction. Biochemistry 30:3105–3114, 1991.
45. Wilschut J, Duzgunes N, Fraley R, Papahadjopoulos D. Studies on the mechanism of membrane fusion: kinetics of calcium ion induced fusion of phosphatidylserine vesicles followed by a new assay for mixing of aqueous vesicle content. Biochemistry 19:6011–6021, 1980.
46. Kelly M, Cho WJ, Jeremic A, Abu-Hamdah R, Jena BP. Vesicle swelling regulates content expulsion during secretion. Cell Biol Int 28:709–716, 2004.
47. Lawson D, Fewtrell C, Gomperts B, Raff M. Anti-immunoglobulin induced histamine secretion by rat peritoneal mast cells studied by immuno ferritin electron microscopy. J Exp Med 142: 391–402, 1975.